



## 3D Voxelisation for Enhanced Environmental Modelling Applications

Nurfairunnajiha Ridzuan<sup>1✉</sup> | Nevil Wickramathilaka<sup>1,2✉</sup> | Uznir Ujang<sup>1</sup> | Suhaibah Azri<sup>1</sup>

1. 3D GIS Research Lab, Faculty of Built Environment and Surveying, Universiti Teknologi Malaysia, Malaysia.

2. Southern Campus, General Sir John Kotelawala Defence University, Edison Hill, Nugegallayaya, Sewanagala, Sri Lanka.

### Article Info

**Article type:**  
Research Article

**Article history:**  
Received: 6 June 2023  
Revised: 23 September 2023  
Accepted: 17 December 2023

**Keywords:**  
*Computational Fluid  
Dynamics  
Three-Dimensional  
Modelling  
Traffic Noise  
Spatial Interpolation  
Voxelisation  
Wind Simulation*

### ABSTRACT

Monitoring and managing environmental problems, particularly those impacting human health such as noise and air pollution, are essential. However, the current implementation has certain limitations that need improvement. In the case of noise pollution, accurately computing noise levels requires considering traffic noise propagating in all directions, necessitating the involvement of a 3D building model. Existing methods using raster cells and noise contours are insufficient in achieving high accuracy. To overcome this, we propose integrating a voxelisation approach and 3D kriging, enabling the depiction of traffic noise values for each voxel. In the context of air pollution, wind movement plays a significant role in the dispersion of contaminants. The current practice involves a random selection procedure for wind simulation within the model discretisation. However, we suggest replacing this randomness with a voxel-based model, which not only improves accuracy but also reduces computing time. Thus, the voxel-based model represents the building model in a wind computation environment, facilitating more realistic wind simulation results. This study demonstrates the applicability of the voxelisation technique in two different environmental modeling contexts using the building model of the city building modeling standard. The level of detail (LoD) in the represented building model differs between these approaches. For traffic noise, a low LoD (LoD1) is sufficient to depict exterior buildings accurately. However, for wind simulation, a higher LoD (LoD2) is necessary to accommodate the complexity of buildings and determine appropriate voxel sizes. In conclusion, the proposed improvements in the form of voxel-based modeling techniques offer enhanced accuracy and efficiency in environmental monitoring. The findings of this study have implications for improving the management and reduction of environmental problems, ultimately benefiting human health and well-being.

**Cite this article:** Ridzuan, N., Wickramathilaka, N., Ujang, U., & Azri, S. (2024). 3D Voxelisation for Enhanced Environmental Modelling Applications. *Pollution*, 10 (1), 151-167.  
<https://doi.org/10.22059/poll.2023.360562.1942>



© The Author(s).

Publisher: The University of Tehran Press.

DOI: <https://doi.org/10.22059/poll.2023.360562.1942>

## INTRODUCTION

Environmental problems are associated with a condition of the law and order that collapsed owing to the intervention of human activities. The frequent occurrence of this problem can degrade the quality of human life. Additionally, with current development, it can induce more impact on the environment and, because of this, it is getting more attention globally in order to address this problem. Pollution events such as noise and air pollution are examples. This issue requires the implementation of a monitoring and observation strategy to control and reduce its impact. With the advancement of computer technology, monitoring can be performed through the modelling of this event digitally, whether in a two-dimensional (2D) or three-dimensional (3D) perspective. However, the applicability of 3D modelling is preferable due to the incorporation of a z-axis that can represent the height of the study area, which can include the impact from different height perspectives and replicate the real-world environment. Because

\*Corresponding Author Email: [nurfairunnajiha2@graduate.utm.my](mailto:nurfairunnajiha2@graduate.utm.my),  
[nevilvidyamaneek@kdu.ac.lk](mailto:nevilvidyamaneek@kdu.ac.lk)

noise and air travel in every direction, 2D raster cells cannot visualise a 3D space. Hence, 3D cells (3D pixels) are useful for visualising traffic noise and wind flow. Thus, a 3D voxel is vital to increase the accuracy and cartographic quality of visualisation (Kurakula and Kaffer, 2008; Konde and Saran, 2017) and improve the implemented technique.

### *Traffic noise and visualisation*

Road traffic noise is the absolute greatest influence on increased noise pollution in urban cities (Huang et al., 2018; Laxmi et al., 2019; Gilani and Mir, 2021). Physical and environmental factors affect traffic noise pollution. Therefore, calculating road traffic noise levels is a complex process. Therefore, to describe the behavior of noise propagation, standard mathematical models are used (Gilani and Mir, 2021). The Henk de Kluijver road traffic noise model is vital to calculate traffic noise (Kurakula and Kaffer, 2008; Ranjbar et al., 2012). The model can be used to predict noise levels in a variety of settings, such as residential neighborhoods, commercial areas, and transportation corridors (Masum et al., 2021; Jasim et al., 2022). However, road traffic noise modeling is a significant tool to assess noise from a large number of sources (Bruguier et al., 2019). Furthermore, road traffic noise modeling is associated with assessing and predicting noise levels through the attributes measured on the ground (Dubey et al., 2022). Traffic noise can travel in all directions, depending on the environment and the magnitude of the noise. In that case, three-dimensional (3D) road traffic noise visualisation embedded with a 3D building model is vital to simulate noise levels where the highest and the measurements that can be observed to mitigate them (Ranjbar et al., 2012; Lee et al., 2022). Noise contours and raster cells are widely used to visualise traffic noise (Kurakula and Kaffer, 2008). However, 3D voxel visualisation of noise is vital to increase the accuracy of visualisation (Kurakula and Kaffer, 2008; Konde and Saran, 2017). Designing noise observation points (Nops) in 3D space, calculating noise levels to Nops, spatial interpolation, and visualisation are prime in road traffic noise voxel modelling (Kurakula and Kaffer, 2008; Li and Heap, 2014).

### *3D kriging and voxels*

A Nop consists of four elements, x-coordinate, y-coordinate, z-coordinate, and a noise value in 3D space (Kurakula and Kaffer, 2008; Jiang et al., 2019). Spatial interpolation such as Inverse Distance Weighted (IDW), Kriging, and Triangular Irregular Networks (TIN) does not support directly interpolating four elements (Chen et al., 2015). However, 3D Kriging provides a significant approach for interpolating four parameters. Furthermore, 3D Kriging is embedded with 3D voxels to visualise road traffic noise (Sukkuea and Heednacram, 2022). Designing Nops in 3D space is vital. In particular, Nops is designed as a grid pattern with the distance between Nops being two metres. Additionally, the same x and y coordinates of Nops should be avoided for z coordinates in the same vertical direction when using IDW, Kriging, and TIN for 3D spatial interpolation. It means that spatial development should be adopted for 3D spatial interpolation (Grunwald et al., 2001). However, in 3D Kriging, these processes should not be applied. Furthermore, 3D Kriging creates geostatistical layers along vertical axes as slices. In addition, the size of the voxels should be small or equal to the resolution of 3D kriging layers (cell sizes). This is the main requirement to produce voxels by 3D kriging layers accurately.

The layers call multidimensional voxel layers and represent multidimensional spatial and temporal data for the 3D volumetric visualisation (Grunwald and Barak, 2003; Lv et al., 2022). Then, these slices and the voxels are designed (Wu et al., 2022). The smaller size of a voxel enhances the accuracy of noise visualisation. The voxel is filled with road traffic noise values of 3D Kriging geostatistical layers (Li et al., 2022). The positional relationship between voxels and the geostatistical layer is vital for this (Madsen et al., 2021). When the voxel is traversed by a geostatistical layer, the positions of cutting points on the voxel edges are computed with respect to the center coordinates of the voxel (Li et al., 2022). Then attributes of these cutting

points can be detected. Based on the attribute values of cutting points and voxel corners, the texture (color) is inserted for the voxel through neighbour interpolation (Mileff and Dudra, 2019). Furthermore, several voxels can be removed or retained when four edges of the voxels are not traversed by a geostatistical layer (Li et al., 2022).

### *Wind flow simulation*

In the study of air pollution, the wind is the element that influences the movement of pollutants (Yang et al., 2020); hence, one of the modelling that can be performed is 3D wind modelling. Wind flow modeling technique utilising Computational Fluid Dynamics (CFD) approach (Moonen et al., 2012; Chatzimichailidis et al., 2019; Gimenez and Bre, 2019; Kaseb et al., 2020; Zheng and Yang, 2021). When dealing with a building-based area, the existence of the building has the ability to manipulate the wind flow, where the building structure becomes the blockage of the flow (Lee and Mak, 2021) and stimulate the flow separation of the wind (Sattar et al., 2018; Rajasekarababu et al., 2019; Juan et al., 2021). The flow separation allows for the production of different wind velocities and patterns. The computation that results in the parameter, such as the velocity, is performed by involving of the Navier-Stokes equation. This equation works along with the turbulence modelling in the simulation domain. Due to irregular molecular fluctuation and mixing, fluids frequently move in turbulent flow in both natural and industrial settings and require the inclusion of turbulence models. One of the models is the Reynolds-Averaged Navier-Stokes (RANS). RANS is preferable for fluid flow simulation since it has lower computational costs and data storage than LES models (Shirzadi et al., 2020). Additionally, another method, the Finite Volume Method (FVM), is used in this simulation (Zhang et al., 2019; Ali et al., 2023). This method solves the Partial Differential Equation (PDE) from the RANS by applying the volume-based concept on domain discretisation. Therefore, all these related computations are conducted within the discretized CFD environment.

### *Simulation and voxels*

A decent wind simulation outcome depends on the model discretisation in the CFD environment. The model discretisation covers all the simulation environment, including the domain with the building model involved, and produces smaller faces for computation purposes. Existing research in this field employs a vector model and performs the discretisation based on the CFD environment itself (Zhang et al., 2020; Zheng et al., 2020; Gaur and Raj, 2022) where it uses the grid independence test (GIT) for the evaluation (Lee et al., 2020; Zhang et al., 2020; Sun et al., 2021). It lacks the specification based on the building modelling concept and aspect. Hence, the voxel approach in generating the building model is introduced to provide the ability of the building model to exist in a voxelised form where the voxel size is used to be represented as the discretisation size of the building model in the wind CFD simulation environment. This voxel size selection depends on the building model representation and detailing. To our knowledge, no implementation of a ready-discretised model is embedded in the CFD domain. Hence, this paper, along with the application of voxel in traffic noise modelling, presents the 3D voxelised structure of a building model to be amalgamated in the CFD environment.

## **METHODS**

This study is carried out to visualise traffic noise in 3D voxels embedded with 3D Kriging and simulate the wind flow using a vectorised building model. The inner circle area of Universiti Teknologi Malaysia (UTM) was selected for these two applications. Additionally, for the noise visualisation application, traffic flow has been identified around several buildings to examine traffic noise levels on building facades. According to a previous study, average noise levels in the study area are 65 dB (A) to 70 dB (A) (Haron et al., 2015).

Regarding wind simulation, the study area provides the reference for generating the building model in the simulation environment in the form of a voxelised model. The location coordinates of the study area are at  $1^{\circ}33'37.6''\text{N}$   $103^{\circ}38'16.4''\text{E}$  and are located at UTM, Johor, Malaysia. Fig. 1 illustrates the overview of the study area.

### *Noise pollution visualisation*

The workflow of the noise pollution study is shown in Fig. 2 below.

Phase 1: Data Acquisition - The 3D building model was designed embedded with the drone points cloud and Geographic Information System (GIS) (see Fig.6). The level of detail (LoD1) is vital to represent 3D buildings in 3D road traffic noise visualisation (Saran et al., 2018). The exterior details of buildings are sufficient, and the walls and roof of a building together design a building. Furthermore, a simplified exterior 3D volume with a flat roof of a building is widely used in 3D traffic noise visualisation (Kumar et al., 2017). Drone point clouds were used to create a 3D building model. When considering statistical data of road, the number of vehicles



**Fig. 1.** Overview of the study area

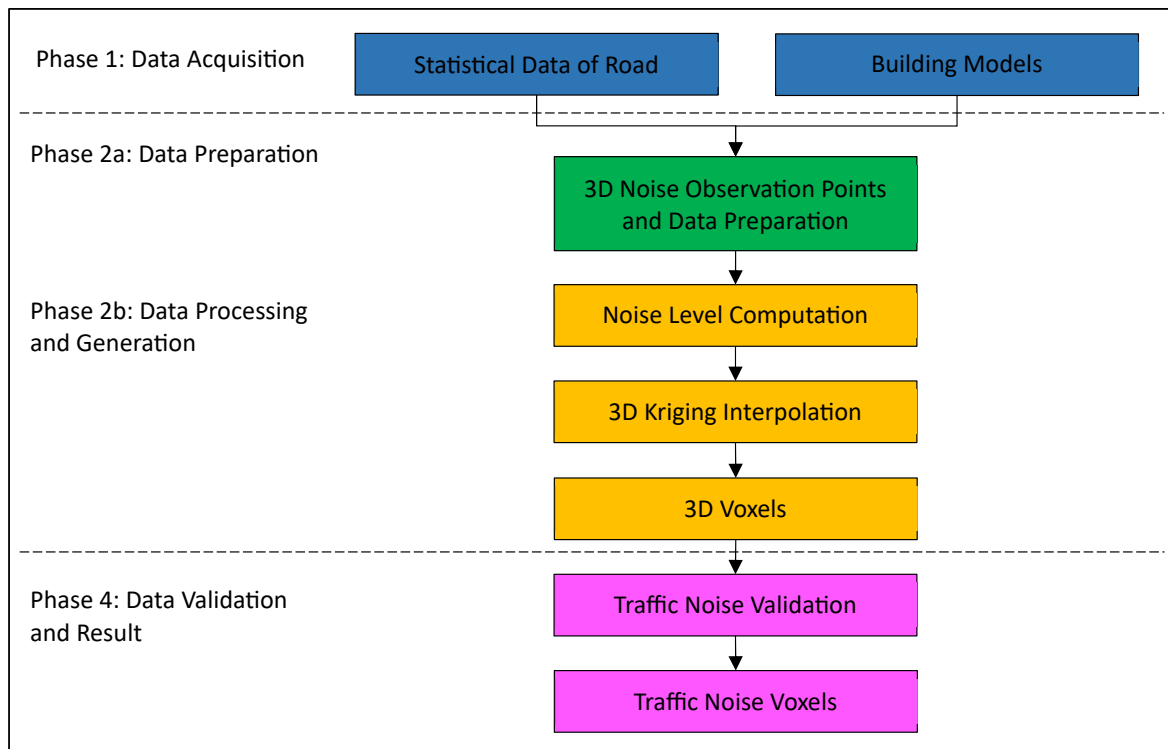


**Fig. 2.** Workflow of the noise pollution study

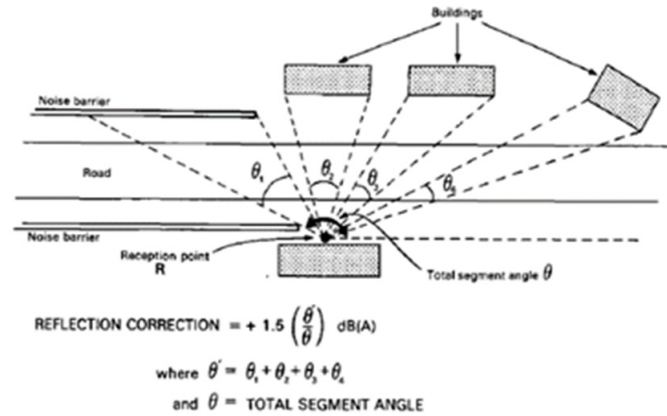


**Fig. 3.** Noise reflection (Hood, 1987)

such as light, medium, and heavy vehicles were counted from 7.30 am to 9.30 am. The speed of vehicles for each category was observed using a vehicle speed meter. The sample of the road traffic noise observations were taken by DEKKO SL-130, sound level meter.

Phase 2a: Data Preparation - The Nops were designed in 3D space along the facades of buildings. The distance interval between Nops is 2 m (Kurakula and Kaffer, 2008). The Nops in 3D space are shown in Fig. 6. The footprints of the buildings and Nops are shown in Fig. 7. For convenience, the buildings were numbered 1-10 (Fig. 9). The Nops were designed on the road segments. Moreover, Nops were not designed along several building facades because opposite facades of same building or other buildings act as noise barriers. Data were prepared according to the Henk de Kluijver road traffic noise model. Equation 1 shows the Henk de Kluijver road traffic noise model (Ranjbar et al., 2012). The model was used to calculate noise levels to Nops. The number of vehicles, types of vehicles, speed of vehicles, noise absorption by ground, noise reflection, weather conditions, and noise barriers are the main factors for road traffic noise pollution (Ranjbar et al., 2012; Mishra et al., 2019).

$$L_{(dB)} = E + C_{optrek} + C_{reflectie} - D_{afstand} - D_{lucht} - D_{bodem} - D_{meteo} - D_{barrier} \quad (1)$$

Where  $L_{(dB)}$  is the traffic noise level.  $E$  is the level of traffic noise emission. To calculate the value of the  $E$  speed of vehicles, the type of vehicle (light, medium, and heavy) and the number of vehicles in the flow of heavy traffic should be observed.  $C_{optrek}$  is the extra noise emission from accelerating and braking.  $C_{reflectie}$  is the noise reflection of barriers and buildings. Moreover, noise reflection can be calculated by Equation 2.

$$C_{reflectie} = 1.5 \times Fobj \quad (2)$$

$Fobj$  is between 0 and 1, and can be calculated from  $(\theta' / \theta)$ . The  $\theta'$  is the sum of the angles subtended from buildings and barriers, and  $\theta$  is the total angle subtended angle (see Fig. 3) (Hood, 1987; Ranjbar, 2012). The reason is, that the buildings are located continuously in the selected area, and the ratio  $\theta'$  and  $\theta$  was assumed to equal 1. Therefore, the noise reflection was taken as 1.5 dB (A).

$D_{afstand}$  is the reduction of noise with distance during propagation. The  $D_{afstand}$  can be calculated by Equation 3. Additionally,  $D_{lucht}$  is the mitigation of traffic noise due to absorption from the air. Equation 4 is shown to calculate the  $D_{lucht}$ . Besides,  $D_{bodem}$  is the traffic noise absorption by ground, and the coefficient of noise absorption by ground (B) is between 0 and 1, presented by Equation 5.

$$D_{afstand} = 10 \log(r) \quad (3)$$

$$D_{lucht} = 0.01 \times r^{0.9} \quad (4)$$

$$D_{bodem} = B + \left[ 2 + 4(1 - e^{-0.04r}) \times \left( e^{-0.65h_w} + e^{-0.65(h_{weg}-0.75)} \right) \right] \quad (5)$$

Where  $r$  is the source of distance between the traffic noise and the receiver (Nop),  $h_w$  is the height of the noise observation point from ground level. The  $h_{weg}$  is the height of the road from the ground level. The ground is completely covered by grass, the  $B$  is 1, and for the hard ground, the  $B$  is 0 (ISO, 1996). When considering the study area of UTM, there is hard ground. Therefore,  $B$  was assumed as 0. Traffic noise mitigation by noise barriers was not considered because there being any wall barriers between buildings and roads. The  $D_{meteo}$  is the mitigation of noise by wind conditions. Furthermore, Equation 6 is shown to calculate  $D_{meteo}$ , where  $e$  is equal to 2.718 (Ranjbar et al., 2012). The  $D_{barrier}$  is reduction of road traffic noise due to wall and building barriers along the roads. When considering this study area there are no noise barriers along roads.

$$D_{meteo} = 3.5 - 3.5e^{(-0.04r/(h_{weg}+h_w+0.75))} \quad (6)$$

Phase 2b: Data Processing and Generation - The 3D Kriging spatial interpolation was applied on Nops to interpolate noise levels. The power variogram was inserted for processing. The 3D Kriging geostatistical layers in 3D space were embedded with voxels to visualise traffic noise pollution on building facades. The size of the voxels was taken as 0.1 m. According to Equation 3, noise reduces approximately 1 dB (A) during 2 m propagation along the horizontal direction and there is no 1 dB (A) noise reduction between two Nops along the vertical direction. However, Nops were designed as a 2 m distance interval along the vertical direction. In this case, a 1 m resolution of 3D kriging geostatistical layers can be combined to 3D voxels which size is 1 m. If the voxel size is 1m, the combined voxel has an irregular appearance. Therefore, to improve the cartographical visualisation quality, 0.1 m 3D kriging geostatistical layers were combined into 0.1 m voxels to visualise road traffic noise pollution in this study. Fig. 9 shows the 3D noise voxel visualisation of the 3D building model and Fig. 10 illustrates the 3D traffic noise voxel visualisation in separate buildings with decibel (dB).

Phase 3: Data Validation and Result - The root mean square error (RMSE) was used to validate the noise levels of the road traffic in 3D space. This study was not focused on visualising road traffic noise inside buildings. Therefore, noise was visualised along the exterior facades of buildings. Nine noise observation points were used to validate the traffic noise visualisation. Sound levels meters were established at corridor of the buildings to observe the actual levels of road traffic noise along facades of the buildings.

#### Wind CFD simulation

The workflow of the wind simulation study is as shown in Fig. 4. In this wind simulation part, two distinct investigations are often conducted. Different arrow colors are used to indicate it, with blue arrows representing for the LoD1-wind simulation and orange arrows representing LoD2 wind simulation. Additionally, this study uses the same building data and model, the LoD1 building model, as the noise pollution study. However, the difference between these two studies is that an additional model is constructed in the wind simulation study, LoD2. The black arrow denotes the application of both studies' use of wind input into the simulation procedure. The vector LoD1 building model is directly incorporated into the CFD simulation process in the LoD 1 wind simulation study, and it goes through a grid independence test to

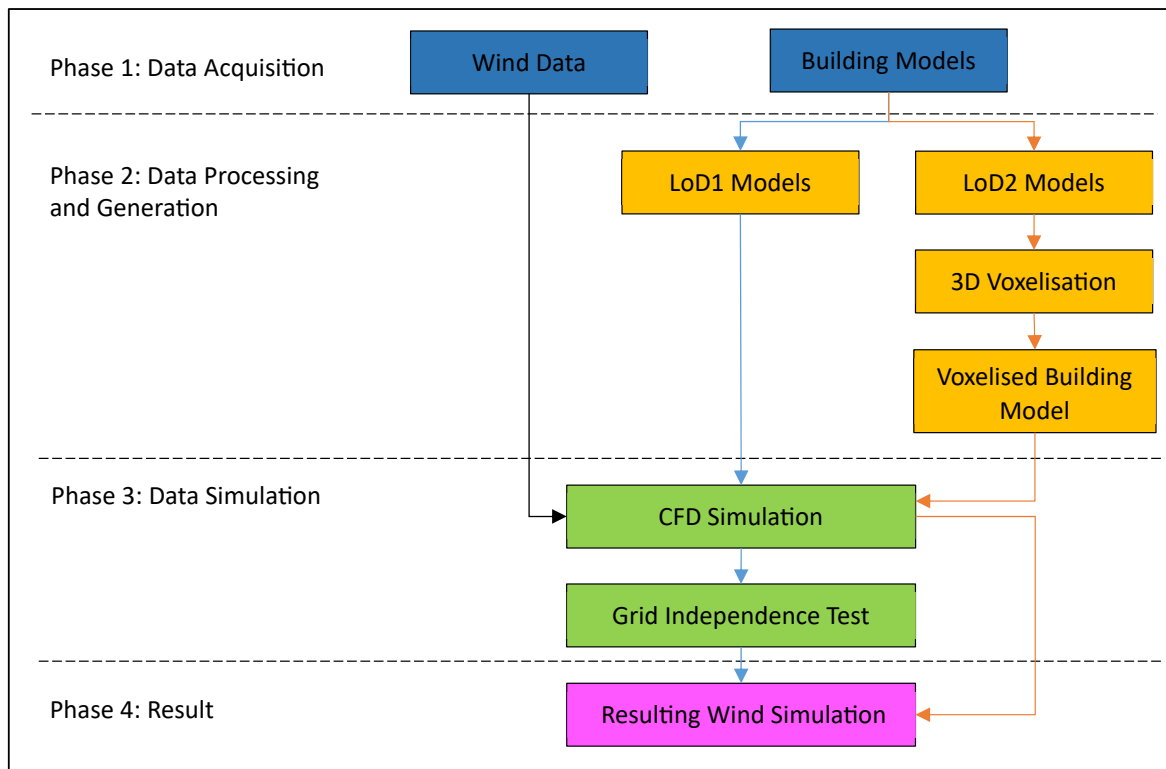


**Fig. 4.** Workflow of the wind simulation study

determine the optimal grid numbering for wind computation (Zhang et al., 2020). In addition, a 3D voxelisation technique is used to convert the model into a voxel-based form (raster form) for the LoD2-wind simulation study. This procedure enables selection of the ideal voxel size for model representation in the simulation domain. The voxelised model later emerges in the simulation environment of the wind calculation process.

Data collection, which includes wind data and building model, is the initial stage. Wind data is the wind velocity of 3 m/s that is fed to the input of the wind simulation domain, and the building model, as previously indicated, is the data gathered by the drone data collection technology. The processing and generation phase involves the LoD1 and LoD2 models. The LoD1 model has a different detailing representation than LoD2 (Kutzner et al., 2020). LoD1 is a building block representation of the study area; while LoD2 adds structures such as roofs and smaller building shapes (Biljecki et al., 2016). Therefore, LoD2 is able to portray a better quality of the building representation. Only the LoD2 model is introduced into the voxelisation process. This is because LoD1 presents a general representation of the building model that cannot provide the suitable sizing reference and deny its ability to be discretised using voxelisation process, while LoD2, with a more detailed structure, allows for voxel size reference in generating the voxel model. The voxel model is constructed using a newly developed integration technique between octree discretisation and duality implementation. The octree introduces the ability for the model to be split into eight nodes, where the higher the depth of the octree, the more nodes exist. However, empty nodes will not be further processed, which can reduce the computation process (Miltiadou et al., 2021). The duality next allows the new voxel model to be generated based on the discretised environment.

In addition, the simulation process is executed by following several standard and implementation. The wind simulation domain (Fig. 5) size is set to 5H for upstream length (lu) and sides (s), 15H for the downstream length (ld), and 6H for the height of the domain (h),

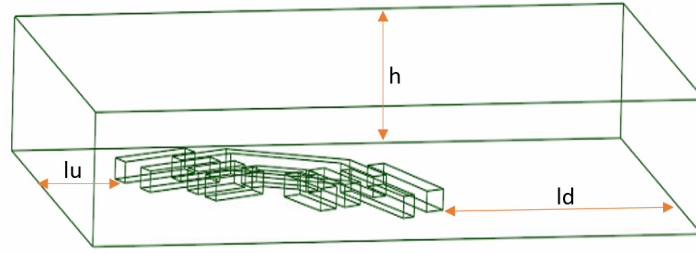


Fig. 5. Wind Simulation Domain

where  $H$  is the height of the building (Franke et al., 2007),  $H = 16.0$  m.

Moreover, this CFD study used the Reynolds Average Navier Stokes (RANS) turbulence model. The RANS equations used the Navier-Stokes equations with applied Reynolds decomposition and separated the parameter values into a sum of the mean and fluctuating components (Blocken, 2018). The equations (Zhang et al., 2020) are as follows.

$$\frac{\partial \bar{u}_i}{\partial x_i} = 0 \quad (7)$$

$$\frac{\partial \bar{u}_i}{\partial t} + \frac{\partial}{\partial x_j} (\bar{u}_i \bar{u}_j) = -\frac{1}{\rho} \frac{\partial \bar{p}}{\partial x_i} + \frac{\partial}{\partial x_j} (2\nu \bar{s}_{ij}) - \frac{\partial}{\partial x_j} (\overline{u'_i u'_j}) \quad (8)$$

$$\frac{\partial \bar{c}}{\partial t} + \frac{\partial}{\partial x_j} (\bar{c} \bar{u}_j) = \frac{\partial}{\partial x_j} \left( D \frac{\partial \bar{c}}{\partial x_j} \right) - \frac{\partial}{\partial x_j} (\overline{c' u'_j}) \quad (9)$$

Where  $u_i$  and  $x_i$  denotes the velocity,  $t$  is time,  $\rho$  is density,  $p$  represents pressure,  $\nu$  is the kinematic viscosity of the fluid,  $c$  denotes the concentration,  $s_{ij}$  is strain-rate tensor and  $(\overline{u'_i u'_j})$  and  $(\overline{c' u'_j})$  refers to the Reynolds stress and turbulence mass.

Furthermore, three distinct CFD environments with various meshing numbers are examined for the grid independence test, which is solely applicable to the LoD1-wind simulation investigation. This is because the vector model is not discretised as in the voxel form. In this study, it is represented by coarse, basic, and fine grids, with the coarse grid having the fewest grids, the basic grid having a medium number, and the fine grid having the most grids. This sensitivity of the grid is assessed by measuring the vertical profile of the wind velocity ( $u$ ), and  $z$  at two different locations: near the closest building from the wind inlet and the center of the study area, 10m and 150m from the domain origin, respectively. The test outcome is displayed as the wind velocity, expressed as  $u/u_{\text{ref}}$  for the x-axis and height,  $z/H$  for the y-axis. The generation of the ensuing wind simulation for both simulation environments using the LoD1 and LoD2 building models brings the investigation to a close.

## RESULTS AND DISCUSSIONS

### 3D noise pollution visualisation

The designed LOD 1 buildings from drone points clouds and noise observation points (Nops) along the facades of the buildings are shown in Fig. 6. The distance interval between Nops is

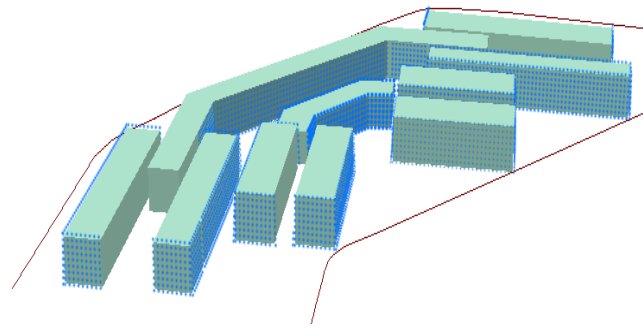


**Fig. 6.** LOD 1 building models and Nops

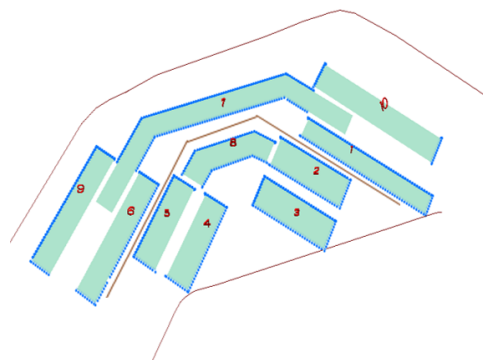


**Fig. 7.** Footprint of buildings and Nops

2m for both vertical and horizontal directions.

In Fig. 7, the footprint of the buildings is represented. Furthermore, the z values of Nops were taken as zero to project the Nops onto 2D. Fig. 8 shows 3D voxels of road traffic noise pollution and 3D kriging road traffic noise geostatistical layers were combined with 3D voxels. The size of the voxel is 0.1 m. Moreover, the 3D voxel road traffic noise visualisation of separate buildings is shown in Fig. 9.

The Henk de Kluijver noise model has been used in this study with modifications. The impact of noise barriers was not considered. Previous studies have formulated an equation to identify noise mitigation by wall barriers. However, there are no wall barriers in this study area. However, several buildings act as noise barriers in this study. As an example, Building 4 acts as a barrier for the front façade of building 5. Thus, Nops were not designed front façade of building 5. The same procedures were adopted if the location of buildings is like that. Moreover, the front facades of buildings act as noise barrier for the back façade of the building. Therefore the, Nops were not designed along the back façade in the same building. To represent the noise traffic noise levels, 3D noise contours, and raster cells are widely used. However, embedding of 3D Kriging with voxels provide higher accurate 3D traffic noise visualisation. The 3D kriging provides infinite multidimensional layers along the vertical direction. After combing these layers, the voxels can be prepared to visualise traffic noise levels. Sample noise observation points were used to calculate the accuracy of voxel the visualisation. The root mean square error (RMSE) was used to validate the visualisation of traffic noise. The RMSE error was 1.081. The size of the voxels was taken as 0.1 m for traffic noise visualisation. The small size of the voxels increases the accuracy of the visualisation. According to the traffic noise model (Henk de Kluijver), the traffic noise levels decrease approximately 1dB for 2-metre propagation in a 2D

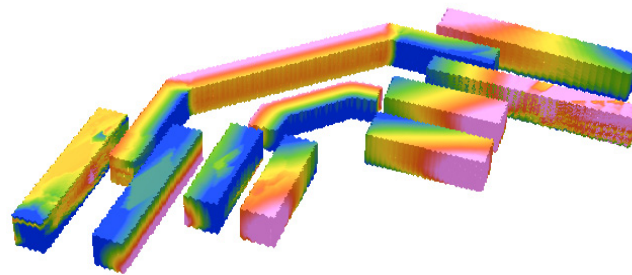


Fig. 8. 3D traffic noise voxels visualisation model

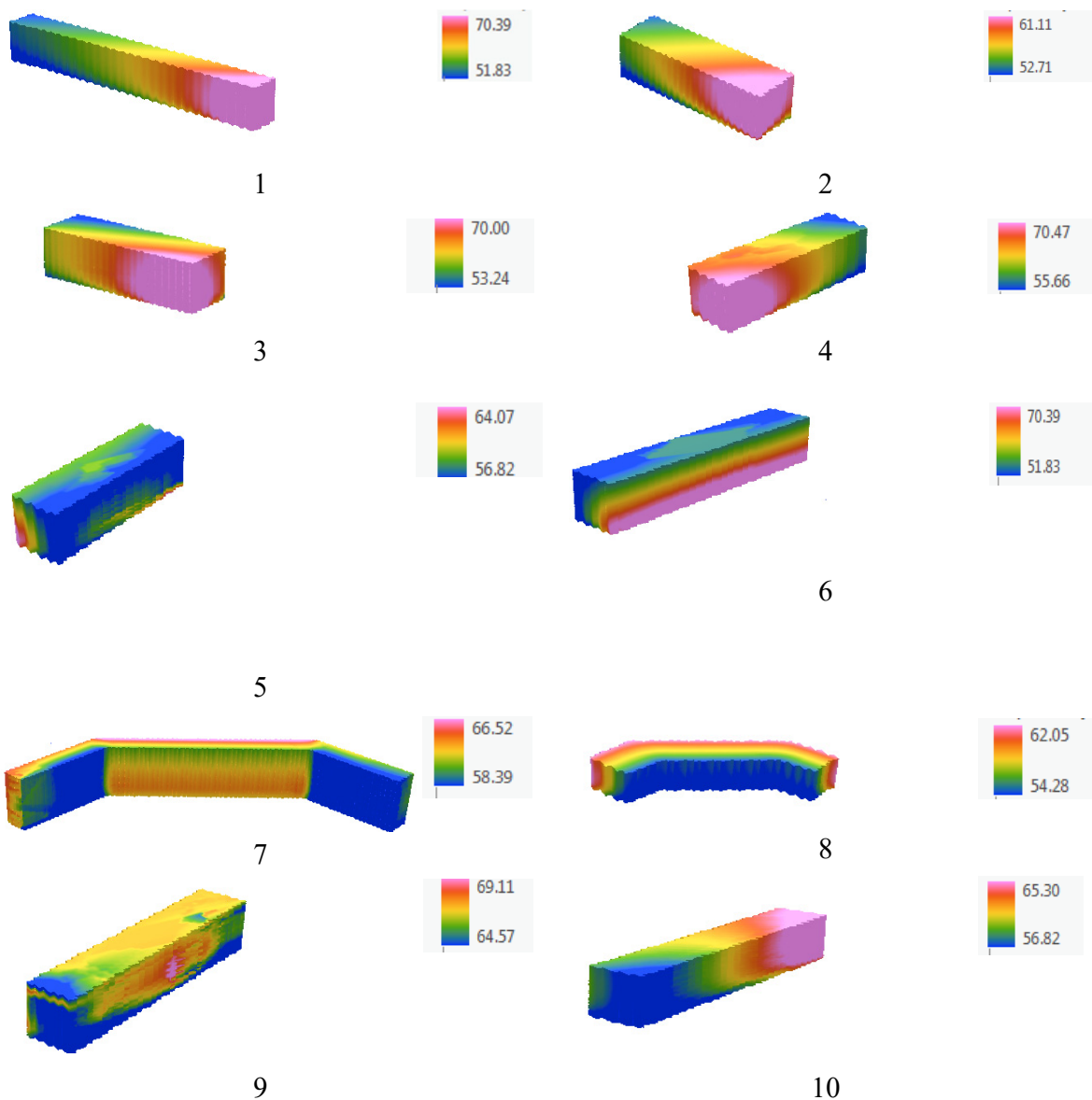
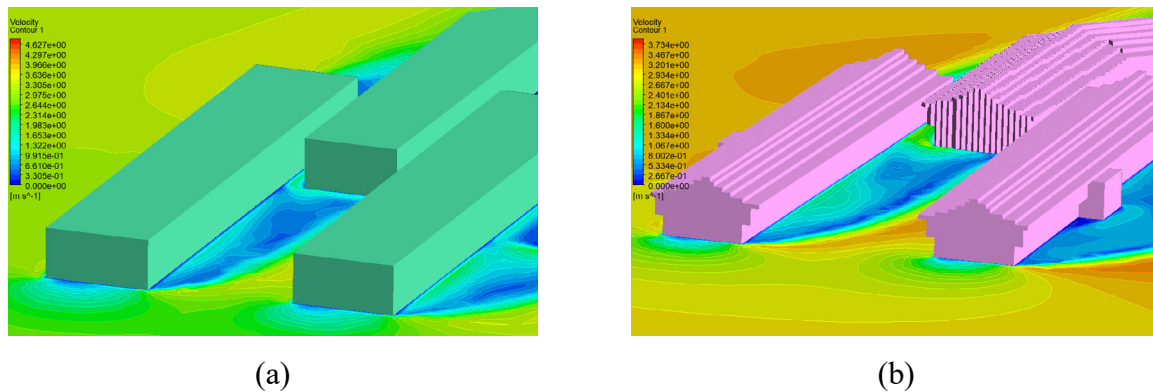


Fig. 9. 3D traffic noise voxels of 3D buildings

space (horizontal direction). However, it reduces approximately 0.4 dB for 2-meter propagation in vertical direction. Therefore, the small size of the voxels (less than 1 metre) is vital for visualizing traffic noise. The 3D kriging is an Empirical Bayesian Kriging, it means that the error of spatial interpolation is computed automatically during the processing. Nop consists of



**Fig. 10.** Wind velocity presented (a) LoD1 model and (b) voxelised LoD2 model

x, y, and z coordinates and a noise value. However, 3D kriging provides facilities to interpolate 4 parameters in 3D space. Thus, embedding 3D kriging multidimensional layers into voxels is vital to increase the accuracy. Other spatial interpolations like Inverse Distance Weighted (IDW), Kriging, and Triangular Irregular Network (TIN) do not provide an accurate spatial interpolation in 3D space, and several developments are needed. The 3D voxel visualisation of traffic noise not only for the noise on the facades, it can be adopted to identify the traffic noise propagation inside the buildings.

### 3D wind CFD simulation

In addition, several results are included in this wind simulation study. Compared to the wind simulation with the LoD2 model (Fig. 12), the LoD1 study goes through a few distinct processes. The LoD1 model, which is embedded in the simulation domain, is discretised to several different meshing as in the grid independence test. The comparison of the coarse, basic, and fine grids used to choose the best meshing type is shown in Fig. 11(a) and (b). Compared to the vertical profile for the coarse grid, the basic and fine grids exhibit comparable vertical profiles and velocity values.

This displays that there is no discernible change in the recorded values. It is feasible to choose a specific type of mesh based on parameter values when fewer meshes than the highest have already reached optimal value (Kummitha et al., 2021). Therefore, the basic grid is chosen as the suitable simulation environment for the integrated wind simulation integrated with LoD1, and the selected wind simulation environment is shown in Fig. 10(a).

In addition to that, the additional building models instead of the LoD1 model, the LoD2 model is shown in Fig. 12(a), which is used in the wind simulation of the LoD2 building model. This LoD2 model is fed as the reference model to generate the voxel-based building model (Fig. 12(b)). The voxel-form representation allows the model to be discretised into smaller volumes in the building generation process. This second simulation environment produces the result of the CFD simulation, as displayed in Fig. 10(b).

The wind simulation outputs from Fig. 10(a) and (b) show the different wind velocity contours, which vary in wind velocity values. It is also associated with the difference in pressure and kinematic energy (Fig. 13 and 14). This is due to the different complexity of the building model (García-Sánchez et al., 2021; Ridzuan et al., 2023), allowing for the formation of recirculation, flow separation, etc., that influence the computed parameter.

According to the workflow in Fig. 4, in the implementation of the process without the voxel technique, the flow requires the execution of the grid independence study. This grid analysis involves the execution of several CFD simulations, where in this study, three different

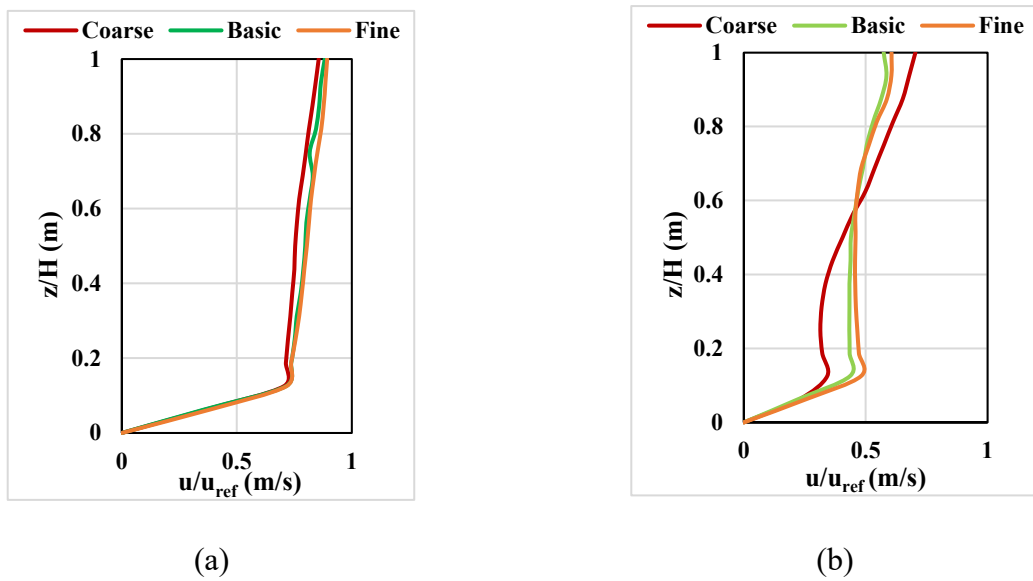


Fig. 11. Grid independence study for LoD1-wind simulation study (a)  $x=10m$  and (b)  $x=150m$

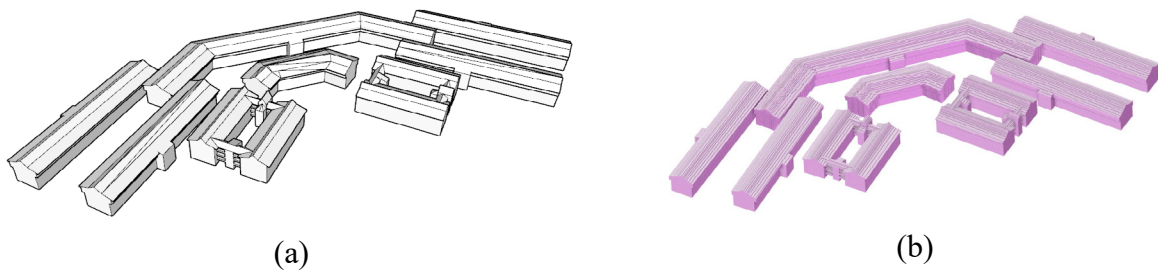


Fig. 12. LoD2 building models (a) Vector form and (b) Raster form

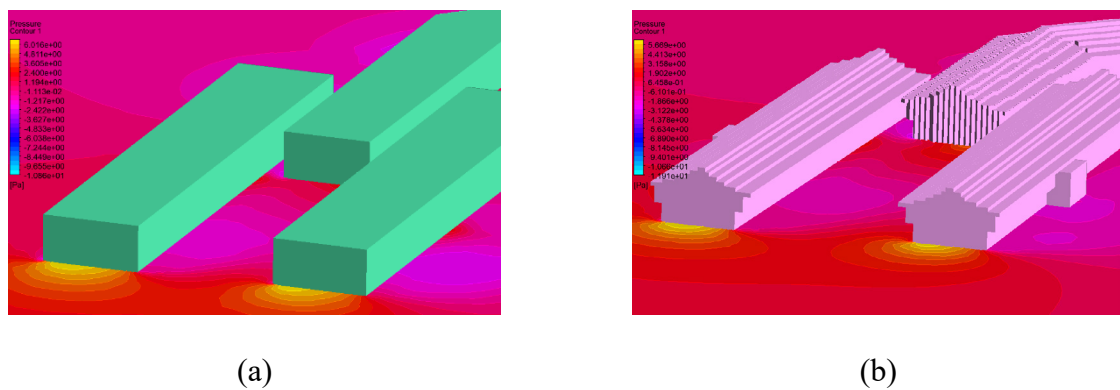
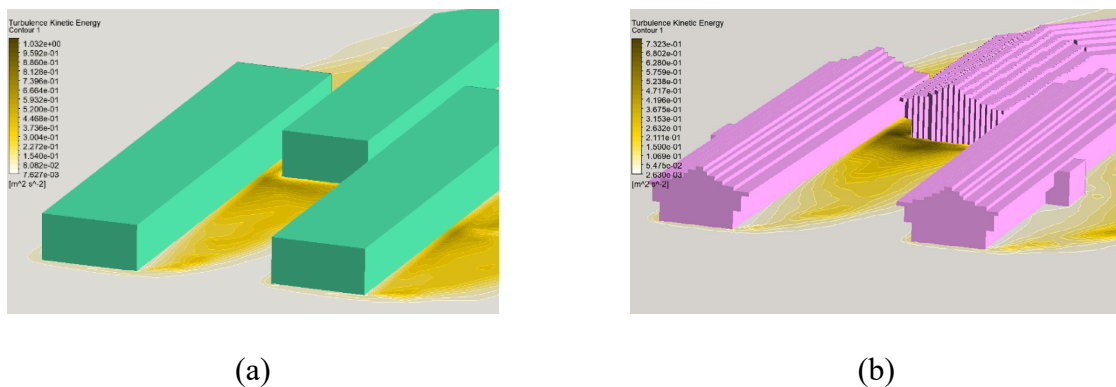


Fig. 13. Wind simulation outputs for pressure representation (a) LoD1 and (b) LoD2

simulations need to be run. These three simulations used various meshing numbers to represent different discretisation complexity: coarse, basic, and fine. However, each of these settings incorporates the same RANS turbulence model, as well as the identical inlet, outlet, and building wall boundary conditions: 3 m/s for the inlet, 0 Pa for the outlet, and nonslip for the building wall boundary. However, this workflow offers random grid selection and requires analysis that can prolong the entire process of producing the wind simulation environment.

Therefore, the simplified procedure can be done with the embedding of the voxel process.



**Fig. 14.** Wind simulation outputs for turbulence kinetic energy representation (a) LoD1 and (b) LoD2

The detailed criterion led to the voxel size of 0.53m being used to discretize the model for wind calculation. The selected sizing allows for a good representation of the building model with complete detailing as from the referred LoD2 model. It is essential to include all the details because the wind simulation process is highly correlated with the shape of the building. Thus, the simulation process with the inclusion of the LoD1 building model requires the grid analysis to get a suitable discretised model, and from the building generation perspective, it can only represent a too general building model. However, implementing the voxelised building model does not require the analysis process where it is already discretised to suit the best building representation and can represent a higher replication of the building model for use in the wind simulation model.

## CONCLUSIONS

Environmental monitoring and control help mitigate the environmental impact on the surrounding. Traffic and air pollution are events that can degrade the quality of the environment. For traffic pollution, focusing on traffic noise mitigation is important for developed and developing cities. To apply precautions to mitigate noise levels, traffic visualisation is vital. Using a proper standard traffic noise model provides an accuracy noise calculation. Embedding 3D Kriging with voxels enhances the accuracy and visual quality of the traffic noise visualisation. The size of the voxels depends on the variation in noise propagation in the horizontal and vertical direction. Understanding the voxel filling process and inserting spatial interpolations for valuing faces of voxel with respect to the centre coordinate is prime to increase the accuracy of voxel visualisation. Generally, nearest-neighbour interpolation is used for voxel filling. Due to 3D kriging provides infinite voxel layers along the vertical axis. Therefore, this spatial interpolation is vital for voxelisation. The visualisation methods and techniques of road traffic noise 3D voxel visualisation can be substituted to visualise air pollution along the facades of buildings in a 3D space. According to the results of road traffic noise visualisation, voxel visualisation can be embedded to elaborate the results of the volumetric information such as geological data model, underground features, and geological features like soil layers and mineral layers. Moreover, to visualise water-related problems like underground water detection and underground water quality management, 3D voxels can be used. In addition, when the value is changed along the vertical direction from the ground surface to underground, 3D kriging spatial interpolation can be accommodated for the voxels. Further, voxel filling through 3D kriging geostatistical layers is needed to be utilised.

Meanwhile, for wind simulation, CFD numerical computation is used to run this simulation.

The current implementation makes use of the grid independence analysis and the vector building concept. However, this elongates the overall process of presenting a suitable simulation environment. The voxelisation approach of constructing a voxel-based model, which exists in discretised form, helps to simplify the whole process without the need to execute the analysis. This was proven by different computed results of LoD1 and voxel-LoD2 environments shown from the representation of velocity, pressure and turbulence kinetic energy value, which mainly influenced by the presented building shape. Hence, the selection of building LoD favors the voxel-LoD2 implementation in the wind simulation environment due to the high correlation of building representation in addition to its capability to support the simplification process of executing the wind simulation. In order to address a variety of applications, this paper introduces the implementation of voxelisation in two distinct environment-related problems. It is concluded that the utilisation of voxelisation in traffic visualisation is to categorize the traffic noise values, and in wind simulation is to produce a building model in voxel form that can support the generation of discretised model for the wind computation purpose. Nonetheless, the execution of wind simulation in relation to the voxelised model can be further studied in terms of the automatic process, where this study only uses a semi-automated approach to generate the voxelised model. In summary, 3D voxels are crucial in these two environmental occurrences. These voxels can be implemented to visualise these incidents and enhance the presented technique. However, the application of the voxelized method is not limited to these two environmental occurrences. The thorough study of this technique can benefit other environmental problems involving 3D space, such as water-related problem and etc.

## **ACKNOWLEDGEMENT**

This research was funded by UTM Research University Grant, Vot Q.J130000.2452.09G84.

## **CONFLICT OF INTEREST**

The authors declare that there is not any conflict of interests regarding the publication of this manuscript. In addition, the ethical issues, including plagiarism, informed consent, misconduct, data fabrication and/ or falsification, double publication and/or submission, and redundancy has been completely observed by the authors.

## **LIFE SCIENCE REPORTING**

No life science threat was practiced in this research.

## **ABBREVIATIONS**

LoD	Level of Detail
2D	Two-Dimensional
3D	Three-Dimensional
IDW	Inverse Distance Weighted
TIN	Triangular Irregular Networks
CFD	Computational Fluid Dynamics
RANS	Reynolds-Averaged Navier Stokes
FVM	Finite Volume Method
GIT	Grid Independence Test

UTM	Universiti Teknologi Malaysia
RMSE	Root Mean Square Error

## REFERENCES

- Ali, M. E., Hasan, M. F., Siddiqa, S., Molla, M. M., & Nasrin Akhter, M. (2023). FVM-RANS modeling of air pollutants dispersion and traffic emission in Dhaka City on a suburb scale. *Sustainability* 2023, 15(1); 673.
- Biljecki, F., Ledoux, H., & Stoter, J. (2016). An improved LOD specification for 3D building models. *Comput. Environ. and Urban Syst.*, 59; 25–37.
- Blocken, B. (2018). LES over RANS in building simulation for outdoor and indoor applications: A foregone conclusion?'. *Build. Simul.*, 11(5); 821–870.
- Brenguier, F., Boué, P., Ben-Zion, Y., Vernon, F., Johnson, C. W., Mordret, A., Coutant, O., Share, P. E., Beaucé, E., Hollis, D., & Lecocq, T. (2019). Train traffic as a powerful noise source for monitoring active faults with seismic interferometry. *Geophys. Res. Lett.*, 46(16); 9529–9536.
- Chatzimichailidis, A. E., Argyropoulos, C. D., Assael, M. J., & Kakosimos, K. E. (2019). Implicit definition of flow patterns in street canyons-recirculation zone-using exploratory quantitative and qualitative methods. *Atmos.*, 10(12); 794.
- Che, D., & Jia, Q. (2019). Three-dimensional geological modeling of coal seams using weighted Kriging method and Multi-Source Data. *IEEE Access*, 7; 118037–118045.
- Chen, C., Hu, K., Li H., Yun A., & Li, B. (2015). Three-dimensional mapping of soil organic carbon by combining kriging method with profile depth function. *PLoS ONE*, 10(6), e0129038.
- Dubey, R., Bharadwaj, S., Sharma, V. B., Bhatt, A., & Biswas, S. (2022). Smartphone-based traffic noise mapping system. *Int. Arch. Photogramm. Remote Sens. Spatial Inf. Sci.*, XLIII-B4-2022; 613–620.
- Franke, J., Hellsten, A., Schlünzen, K. H., & Carissimo, B. (2007). Best practice guideline for the CFD simulation of flows in the urban environment-a summary. In 11th Conf. on Harmonisation within Atmospheric Dispersion Modelling for Regulatory Purposes, Cambridge, UK, July 2007 Cambridge Environmental Research Consultants.
- García-Sánchez, C., Vitalis, S., Paden, I., & Stoter, J. (2021). The impact of level of detail in 3D city models for CFD-based wind flow simulations. *Int. Arch. Photogramm. Remote Sens. Spatial Inf. Sci.*, XLVI-4/W4; 67–72.
- Gaur, N., & Raj, R. (2022). Aerodynamic mitigation by corner modification on square model under wind loads employing CFD and wind tunnel. *Ain Shams Eng. J.*, 13(1); 101521.
- Gilani, T. A., & Mir, M. S. (2021). Modelling road traffic noise under heterogeneous traffic conditions using the graph-theoretic approach. *Environ. Sci. Pollut. Res.*, 28(27); 36651–36668.
- Gimenez, J. M., & Bre, F. (2019). Optimization of RANS turbulence models using genetic algorithms to improve the prediction of wind pressure coefficients on low-rise buildings. *J. Wind Eng. Ind. Aerodyn.*, 193; 103978.
- Grunwald, S., & Barak, P. (2003). 3D geographic reconstruction and visualization techniques applied to land resource management. *Trans. in GIS*, 7(2); 231–241.
- Grunwald, S., Barak, P., & Rooney, D. (2001). Web-based virtual models for the earth science community. *Am. Soc. Agric. Eng.*, 2001; 1-9.
- Haron, Z., Ming Han, L., Darus, N., Ling Lee, Y., Jahya, Z., Abdul Hamid, M. F., Yahya, K., & Ngian Shek, P. (2015). A preliminary study of environmental noise in public university. *J. Teknol.*, 77(16); 145–151.
- Hood, R. A. (1987). Accuracy of calculation of road traffic noise. *Appl. Acoust.*, 21; 139–146.
- Huang, Y., Wang, L., Hou, Y., Zhang, W., & Zhang, Y. (2018). A prototype IOT based wireless sensor network for traffic information monitoring. *Int. J. Pavement R. Technol.*, 11(2); 146–152.
- ISO 9613-2. (1996). Acoustics – Attenuation of sound during propagation outdoors – Part 2: General method of calculation
- Jasim, S. A., Rudiansyah, M., Ongdashkyzy, O. A., Taban, T. Z., Chupradit, S., Iswanto, A. H., Suhayb, M. K., Falih, K. T., Alshahrani, N. Z., & Mustafa, Y. F. (2022). Determining the parameters of noise pollution in the central area of the Almaty city in Kazakhstan. *Noise Mapp.*, 9(1); 120–127.
- Jiang, Q., Peng, J., Biswas, A., Hu, J., Zhao, R., He, K., & Shi, Z. (2019). Characterising dryland salinity in three dimensions. *Sci. Total Environ.*, 682; 190–199.

- Juan, Y. H., Wen, C. Y., Li, Z., & Yang, A. S. (2021). Impacts of urban morphology on improving urban wind energy potential for generic high-rise building arrays. *Appl. Energy*, 299; 117304.
- Kaseb, Z., Hafezi, M., Tahbaz, M., & Delfani, S. (2020). A framework for pedestrian-level wind conditions improvement in urban areas: CFD simulation and optimization. *Build. Environ.*, 184; 107191.
- Konde, A., & Saran, S. (2017). Web-enabled spatiotemporal semantic analysis of traffic noise using CityGML. *J. Geomat.*, 11(2); 248–259.
- Kumar, K., Ledoux, H., Commandeur, T. J. F., & Stoter, J. E. (2017). Modelling urban noise in City GML ADE: case of the Netherlands. *ISPRS Ann. Photogramm. Remote Sens. Spat. Inf. Sci.*, 4(4W5); 73–81.
- Kummitha, O. R., Kumar, R. V., & Krishna, V. M. (2021). CFD analysis for airflow distribution of a conventional building plan for different wind directions. *J. Comput. Des. Eng.*, 8(2); 559–569.
- Kurakula, V. K., & Kuffer, M. (2008). 3D noise modeling for urban environmental planning and management. *CORP 008: Mobility Nodes as Innovation Hubs: Proc. 13th Int. Conf. Urban Planning Reg. Dev. Inf. Society*, Vienna, May 19–21 2008, Competence Center of Urban and Regional Planning, Schwechat 2008, 517–523
- Kutzner, T., Chaturvedi, K., & Kolbe, T. H. (2020). CityGML 3.0: New functions open up new applications. *J. Photogramm. Remote Sens. Geoinf. Sci.*, 88(1); 43–61.
- Laxmi, V., Dey, J., Kalawapudi, K., Vijay, R., & Kumar, R. (2019). An innovative approach of urban noise monitoring using cycle in Nagpur, India. *Environ. Sci. Pollut. Res.*, 26(36); 36812–36819.
- Lee, H. M., Luo, W., Xie, J., & Lee, H. P. (2022). Traffic noise reduction strategy in a large city and an analysis of its effect. *Appl. Sci.*, 12(12); 6027.
- Lee, K. Y., & Mak, C. M. (2021). Effects of wind direction and building array arrangement on airflow and contaminant distributions in the central space of buildings. *Build. Environ.*, 205; 108234.
- Lee, M., Park, G., Park, C., & Kim, C. (2020). Improvement of grid independence test for computational fluid dynamics model of building based on grid resolution. *Adv. Civ. Eng.*, 2020; 8827936.
- Li, J., Liu, P., Wang, X., Cui, H., & Ma, Y. (2022). 3D geological implicit modeling method of regular voxel splitting based on layered interpolation data. *Sci. Rep.*, 12(1); 1–14.
- Li, J., & Heap, A. D. (2014). Spatial interpolation methods applied in the environmental sciences: A review. *Environ. Model. Softw.*, 53, 173–89.
- Lv, T., Fu, J., & Li, B. (2022). Design and application of multi-dimensional visualization system for large-scale ocean data. *ISPRS Int. J. Geo-Information*, 11(9); 491.
- Madsen, R. B., Kim, H., Kallesøe, A. J., Sandersen, P. B. E., Vilhelmsen, T. N., Hansen, T. M., Christiansen, A. V., Møller, I., & Hansen, B. (2021). 3D multiple-point geostatistical simulation of joint subsurface redox and geological architectures. *Hydrol. Earth Syst. Sci.*, 25(5); 2759–2787.
- Masum, M. H., Pal, S. K., Akhie, A. A., Ruva, I. J., Akter, N., & Nath, S. (2021). Spatiotemporal monitoring and assessment of noise pollution in an urban setting. *Environ. Chall.*, 5; 100218.
- Mileff, P., & Dudra, J. (2019). Simplified voxel based visualization. *Prod. Syst. Inf. Eng.*, 8; 5–18.
- Miltiadou, M., Campbell, N. D. F., Cosker, D., & Grant, M. G. (2021). A comparative study about data structures used for efficient management of voxelised full-waveform airborne LiDAR data during 3D polygonal model creation. *Remote Sens.* 2021, 13(4); 559.
- Mishra, R. K., Mishra, A. R., & Singh, A. (2018). Traffic noise analysis using RLS-90 model in urban city. *INTER-NOISE and NOISE-CONgr. Conf. Proc.*, 259(3); 6490-6502.
- Moonen, P., Defraeye, T., Dorer, V., Blocken, B., & Carmeliet, J. (2012). Urban Physics: Effect of the micro-climate on comfort, health and energy demand. *Front. Archit. Res.*, 1(3); 197–228.
- Rajasekarababu, K. B., Vinayagamurthy, G., & Selvi Rajan, S. (2019). Experimental and computational investigation of outdoor wind flow around a setback building. *Build. Simul.*, 12(5); 891–904.
- Ranjbar, H. R., Gharagozlou, A. R., & Vafaei Nejad, A. R. (2012). 3D analysis and investigation of traffic noise impact from Hemmat Highway located in Tehran on buildings and surrounding areas. *J. Geogr. Inf. Sys.*, 4(4); 322-334.
- Ridzuan, N., Ujang, U., & Azri, S. (2023). 3D vectorization and rasterization of CityGML standard in wind simulation. *Earth Sci. Informatics*, 16(3); 2635-2647.
- Saran, S., Oberai, K., Wate, P., Konde, A., Dutta, A., Kumar, K., & Senthil Kumar, A. (2018). Utilities of virtual 3D city models based on CityGML: various use cases. *J. Indian Soc. Remote Sens.*, 46(6); 957–972.
- Sattar, A. M. A., Elhakeem, M., Gerges, B. N., Gharabaghi, B., & Gultepe, I. (2018). Wind-induced

- air-flow patterns in an urban setting: Observations and numerical modeling. *Pure Appl. Geophys.*, 175(8); 3051–3068.
- Shirzadi, M., Mirzaei, P. A., & Tominaga, Y. (2020). RANS model calibration using stochastic optimization for accuracy improvement of urban airflow CFD modeling. *J. Build. Eng.*, 32; 101756.
- Sukkuea, A., & Heednacram, A. (2022). Prediction on spatial elevation using improved kriging algorithms: An application in environmental management. *Expert Syst. Appl.*, 207; 117971.
- Sun, D., Shi, X., Zhang, Y., & Zhang, L. (2021). Spatiotemporal distribution of traffic emission based on wind tunnel experiment and computational fluid dynamics (CFD) simulation. *J. Clean. Prod.*, 282; 124495.
- Wickramathilaka, N., Ujang, U., Azri, S., & Choon, T. L. (2023a). Calculation of road traffic noise, development of data, and spatial interpolations for traffic noise visualization in three-dimensional space. *Geomat. Environ. Eng.*, 17(5), 61–85.
- Wickramathilaka, N., Ujang, U., Azri, S., & Choon, T. L. (2023b). Three-dimensional visualisation of traffic noise based on the Henk de-Kluyjver Model. *Noise Mapp.*, 10(1).
- Wu, H., Zhu, Q., Guo, Y., Zheng, W., Zhang, L., Wang, Q., Zhou, R., Ding, Y., Wang, W., Pirasteh, S., & Liu, M. (2022). Multi-level voxel representations for digital twin models of tunnel geological environment. *Int. J. Appl. Earth Obs. Geoinf.*, 112; 102887.
- Yang, J., Shi, B., Shi, Y., Marvin, S., Zheng, Y., & Xia, G. (2020). Air pollution dispersal in high density urban areas: Research on the triadic relation of wind, air pollution, and urban form. *Sustain. Cities Soc.*, 54; 101941.
- Zhang, M., Bae, W., & Kim, J. (2019). The effects of the layouts of vegetation and wind flow in an apartment housing complex to mitigate outdoor microclimate air temperature. *Sustainability* 2019, 11(11); 3081.
- Zhang, X., Weerasuriya, A. U., & Tse, K. T. (2020). CFD simulation of natural ventilation of a generic building in various incident wind directions: Comparison of turbulence modelling, evaluation methods, and ventilation mechanisms. *Energy Build.*, 229, 110516.
- Zheng, X., Montazeri, H., & Blocken, B. (2020). CFD simulations of wind flow and mean surface pressure for buildings with balconies: Comparison of RANS and LES. *Build. Environ.*, 173; 106747.
- Zheng, X., & Yang, J. (2021). CFD simulations of wind flow and pollutant dispersion in a street canyon with traffic flow: Comparison between RANS and LES. *Sustain. Cities Soc.*, 75; 103307.